NUREG/CR-0640
ORNL/SUB/7015-2
DIST. CATEGORY NRC-5

COLLEGE OF ENGINEERING

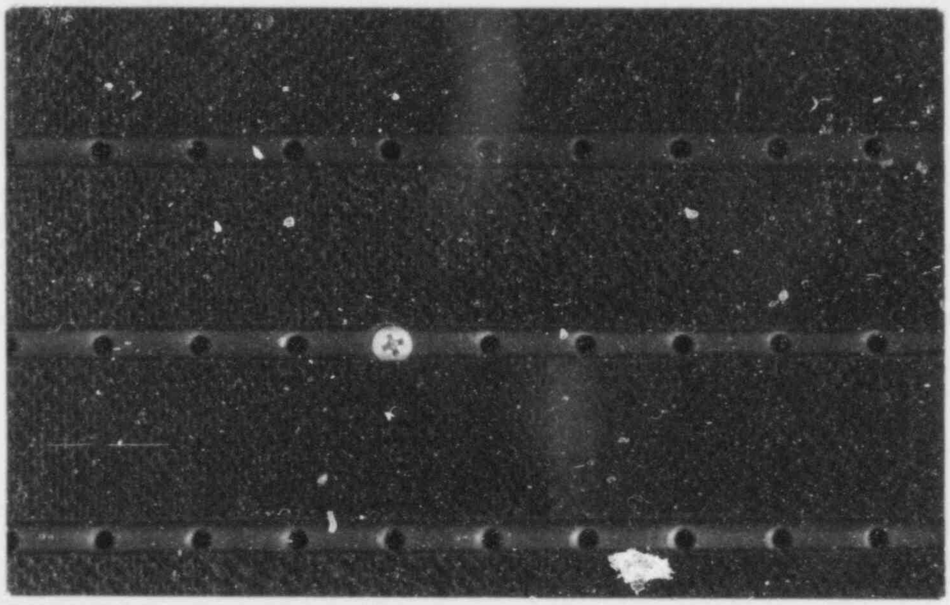

VIRGINIA POLYTECHNIC INSTITUTE AND STATE UNIVERSITY

BLACKSBURG, VIRGINIA

7908140068

648 085

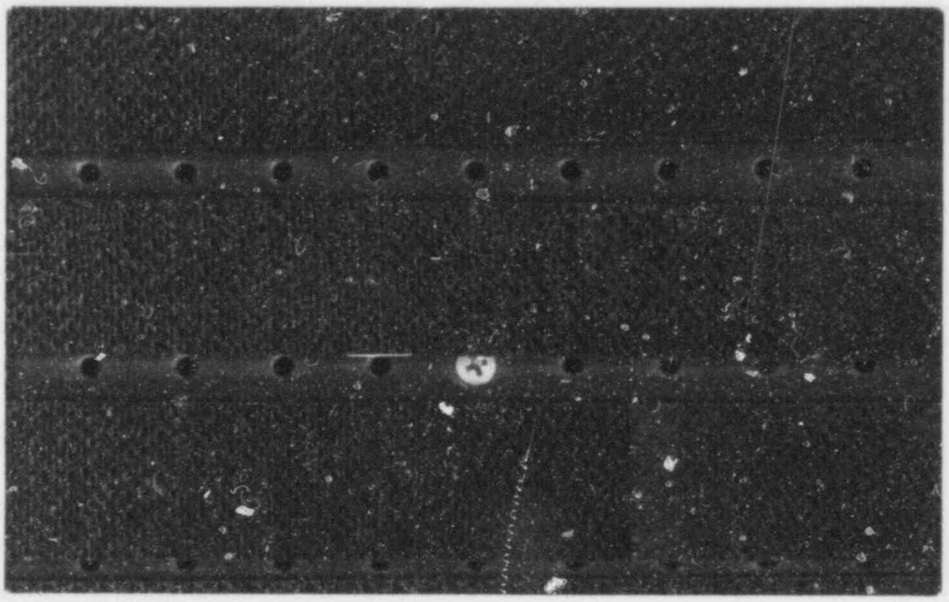

Printed in the United States of America available from:
National Technical Information Service
U.S. Department of Commerce
5285 Port Royal Road
Springfield, VA 22161
Price: Printed Copy — $4.00
Microfiche — 2.25

Report prepared by:
Department of Engin ring Science & Mechanics
College of Engineering
Virginia Polytechnic Institute and State University
Blacksburg, VA 24061
under subcontract number 7015

NUREG/CR-0640
ORNL/sub-7015/2
Dist. Category R5

VPI-E-79-2 January 1979

STRESS INTENSITY DISTRIBUTIONS IN NOZZLE CORNER CRACKS OF COMPLEX GEOMETRY

C. W. Smith, Professor
W. H. Peters, Assistant Professor
W. T. Hardrath, Instructor
T. S. Fleischman, Pratt Research Assistant

Department of Engineering Science and Mechanics

January 1979

Work funded by
U.S. Nuclear Regulatory Commission
Office of Nuclear Regulatory Research
Under Interagency Agreements 40-551-75 and 40-552-75
NRC FIN No. B0119

Prepared for
OAK RIDGE NATIONAL LABORATORY
Oak Ridge, Tennessee 37830
operated by
UNION CARBIDE CORPORATION
for the
DEPARTMENT OF ENERGY

Contract No. W-7405-eng-26

648 087

1. Report No.

VPI-E-79-2

2. Government Accession No.

NUREG/CR-0640

3. Recipient's Catalog No.

ORNL/Sub /7015-2

4. Title:

STRESS INTENSITY DISTRIBUTIONS IN NOZZLE CORNER CRACKS OF COMPLEX GEOMETRY

5. Report Date

January 1979

7. Authors

C. W. Smith, W. H. Peters, W. T. Hardrath, T. S. Fleischman

8. Performing Organization Report Number

VPI-E-79-2

9. Performing Organization Name & Address

Department of Engineering Science & Mechanics
Virginia Polytechnic Institute & State Univeristy
Blacksburg, Virginia 24061

10. Work Unit

VPI-808916-1,2

12. Sponsoring Agency Name and Address

Union Carbide Corporation
Oak Ridge, TN 37830

11. Contract or Grant No.

Sub-Contract No. 7105-
Under W-7405-ENG-26

13. Type of Report & Period Covered

11/1/76 - 12/31/78

16. Abstract

A series (14 models, 28 nozzles) of frozen stress photoelastic experiments were conducted on scale models of boiling water reactor vessels each containing two diametrically opposite cracked nozzles with cracks oriented at 0°, 45° or 90° to the plane on which the vessel hoop stress acted. A range of flaw sizes were studied and cracks were extended by internal pressure loading. Flaw shapes and Stress Intensity Factor (SIF) distributions were obtained and average values of the latter were compared with analytical results. Results suggest that:

i) Flaw growth is non-self-similar and SIF distributions are sensitive to flaw shapes.

ii) When loaded by shear modes, flaws reorient themselves often forming non-planar cracks so as to eliminate the shear mode.

Quantitative flaw shapes and SIF distributions are provided.

17. Key Words

Photoelasticity, Nozzle Cracks, Stress Intensity Factors, Fracture Mechanics, Pressure Vessels

18. Distribution Statement

Approved for Public Release; Distribution Unlimited

19. Security Classification (report)

Unclassified

20. Security Classif. (page)

Unclassified

648 088

FOREWORD

VIRGINIA POLYTECHNIC INSTITUTE AND STATE UNIVERSITY

Blacksburg, VA 24061

The work reported here was performed under sponsorship of the U.S. Nuclear Regulatory Commission (NRC) Heavy-Section Steel Technology (HSST) Program, which is directed by (ORNL). The program is conducted as part of the ORNL Pressure Vessel Technology Program, of which G. D. Whitman is manager. The manager for the NRC is C. Z. Serpan, Jr.

This report is designated Heavy-Section Steel Technology Program or Programmatic Technical Manuscript No. 31. Prior reports in this series are listed below.

1. A Guide for Material Control and Data Control for the Heavy Section Steel Technology Program, Oak Ridge National Laboratory, June 15, 1968 (prepared by ORNL Inspection Engineering Department).
2. C. L. Segaser, System Design Description of the Intermediate Vessel Tests for the Heavy Section Steel Technology Program, USAEC Report ORNL-TM-2849, Revised, Oak Ridge National Laboratory, July 1973.
3. HSST Intermediate Vessel Closure Analysis, Teledyne Materials Research Company, Waltham, Massachusetts, Technical Report E-1253(b), March 25, 1970.
4. C. L. Segaser, Feasibility Study, Irradiation of Heavy Section Steel Specimens in the South Tests Facility of Oak Ridge Research Reactor, USAEC Report ORNL-TM-3234, Oak Ridge National Laboratory, May 1971.
5. D. A. Canonico, Transition Temperature Considerations for Thick-Wall Nuclear Pressure Vessels, USAEC Report ORNL-TM-3114, Oak Ridge National Laboratory, October 1970.
6. F. J. Witt and R. G. Berggren, Size Effects and Energy Disposition in Impact Specimen Testing of ASTM A 533 Grade B Steel, USAEC Report ORNL-TM-3030, Oak Ridge National Laboratory, August 1970.
7. G. D. Whitman and F. J. Witt, Heavy Section Steel Technology Program, USAEC Report ORNL-TM-3055, Oak Ridge National Laboratory, November 1970.

8. D. A. Canonico and R. G. Berggren, Tensile and Impact Properties of Thick-Section Plate and Weldments, USAEC Report ORNL-TM-3211, Oak Ridge National Laboratory, January 1971.

9. J. G. Merkle, L. F. Kooistra and R. W. Derby, Interpretations of the Drop Weight Test in Terms of Strain Tolerance (Gross Strain) and Fracture Mechanics, USAEC Report ORNL-TM-3247, Oak Ridge National Laboratory, June 1971.

10. J. G. Merkle, A Review of Some of the Existing Stress Intensity Factor Solutions for Part-Through Surface Cracks, USAEC Report ORNL-TM-3983, Oak Ridge National Laboratory, January 1973.

11. N. Krishnamurthy, Three-Dimensional Finite Element Analysis of Thick-Walled Vessel-Nozzle Junctions with Curved Transitions, USAEC Report ORNL-TM-3315, Oak Ridge National Laboratory, July 1971.

12. C. E. Childress, Manual for ASTM A-533 Grade B Class 1 Steel (HSST Plate 03) Provided to the International Atomic Energy Agency, USAEC Report ORNL-TM-3193, Oak Ridge National Laboratory, March 1971.

13. G. C. Robinson, Discussion of SwRI Model Parametric Tests, USAEC Report ORNL-TM-3313, Oak Ridge National Laboratory, June 1971.

14. F. J. Witt, The Equivalent Energy Method for Calculating Elastic-Plastic Fracture, October 1973 (Unpublished).

15. R. W. Derby and C. L. Segaser, Quality Assurance Program Plan, Intermediate Vessel Test Facility (HSST Program), USAEC Report ORNL-TM-3373, Oak Ridge National Laboratory, May 1971.

16. C. W. Hunter and J. A. Williams, Fracture and Tensile Behavior of Neutron-Irradiated A533-B Pressure Vessel Steel, Hanford Engineering Development Laboratory, Richland, Washington, Report No. HEDL-TME 71-76, February 6, 1971.

17. A. A. Abbatiello and R. W. Derby, Notch Sharpening in a Large Tensile Specimen by Local Fatigue, USAEC Report ORNL-TM-3925, Oak Ridge National Laboratory, November 1972.

18. S. A. Legge, Effects on Fracture Mechanics Parameters of Displacement Measurement Geometry for Varying Specimen Sizes, Westinghouse Electric Corporation, Pittsburgh, Pennsylvania, Report No. WCAP-7926, June 1972.

19. F. J. Witt and T. R. Mager, A Procedure for Determining Bounding Values on Fracture Toughness K_{Ic} at Any Temperature, USAEC Report ORNL-TM-3894, Oak Ridge National Laboratory, October 1972.

20. J. G. Merkle, An Elastic-Plastic Thick-Walled Hollow Cylinder Analogy for Analyzing the Strains in the Plastic Zone Just Ahead of a Notch Tip, USAEC Report ORNL-TM-4071, Oak Ridge National Laboratory, January 1973.

648 090

21. K. K. Klindt and D. A. Canonico, Evaluation of Discontinuities in HSST Twelve-Inch-Thick Plate, USAEC Report ORNL-TM-4155, Oak Ridge National Laboratory, June 1973.

22. S. A. Legge, Analysis and Experimental Verification of the Thermal Behavior of a Four Inch Steel Section Undergoing Nuclear Heating, Westinghouse Electric Corporation, Pittsburgh, Pennsylvania, Report No. WCAP-8022, December 1972.

23. R. W. McClung, K. K. Klindt and K. V. Cook, An Evaluation of the PVRC and EEI-TVA Programs for Pre- and In-Service Nondestructive Examination of Nuclear Pressure Vessels, June 1973. (Unpublished)

24. G. C. Robinson, J. G. Merkle and R. W. Derby, Fracture Initiation Aspects of the Loss of Coolant Accident for Water Cooled Nuclear Reactor Pressure Vessels, September 1973 (Unpublished).

25. W. K. Wilson and J. A. Begley, Variable Thickness Study of the Edge Cracked Bend Specimen, Westinghouse Electric Corporation, Pittsburgh, Pennsylvania, Report No. WCAP-8237, November 1973.

26. J. A. Williams, Some Comments Related to the Effect of Rate on the Fracture Toughness of Irradiated ASTM A533-B Steel Based on Yield Strength Behavior, HEDL-SA 797, December 1974.

27. S. C. Grigory, Heavy Section Steel Program Tests of 6-Inch-Thick Tensile Specimens Sixth Technical Summary Report, Southwest Research Institute, San Antonio, Texas, SwRI Project 03-2520, April 19, 1974.

28. H. J. Bellucci, Three-Diemnsional Elastic-Plastic Stress and Strain Analyses for Fracture Mechanics: Complex Geometries, MARC Analysis Research Corporation, Palo Alto, CA, Report No. 09177 (TR 75), November 1975.

29. Richard Smith, Weld Repair of Heavy Section Steel Technology Program Vessel V-7, Electric Power Research Institute, Palo Alto, California, EPRI NP-179 (ORNL/Sub/88242-76/1) August 1976, prepared by Combustion Engineering, Inc., Chattanooga, Tennesse, W. D. Goins and D. L. Butler).

30. C. W. Smith, M. Jolles and W. H. Peters, Stress Intensitites for Nozzle Cracks in Reactor Vessels, VPI-E-76-25, Virginia Polytechnic Institute and State University, Blacksburg, Virginia, November 1976.

TABLE OF CONTENTS

Nomenclature

n,t,z	Local rectangular cartesian coordinates along the flaw border (mm)
σ_{ij} i,j = n,z	Stress components in plane normal to the flaw surface and flaw border near crack tip (kPa)
σ_{ij}^{o} i,j = n,z	Part of regular stress field near crack tip (kPa)
r, Θ	Polar coordinates, measured from crack tip (mm,rad)
K_I	Mode I - Stress Intensity Factor (kPa-$m^{1/2}$) (SIF)
K_{AP}	Mode I - Apparent Stress Intensity Factor $[\tau_{max}(8\pi r)^{1/2}]$ (kPa-$m^{1/2}$)
N	Stress fringe order
f	Material fringe value (N/m)
t'	Slice thickness (mm)
p	Internal Pressure (kPa)
α	Angle of rotation from point of flaw intersection with vessel wall (degrees) 0° flaw orientation
β	Angle of rotation from nozzle to point on flaw border 90° flaw orientation
a	Flaw depth at α = 45° or β = 45° (mm)
T	Vessel wall thickness at α = 45° or β = 45° (mm)
a_V	Flaw depth along vessel wall (mm)
a_N	Flaw depth along nozzle wall (mm)
r_z	Inside nominal radius of the nozzle (mm)
ν	Poisson's ratio
γ	Figure 11a
τ_{max}	Maximum in plane shearing stress (kPa)
A	$K_I/\sqrt{8\pi}$
B	A function of regular stresses σ_{ij}^{0}
q	Load parameter

$\bar{\sigma}$	Uniform stress (kPa)
a*	A particular value of flaw depth (mm)
β_{max}	Angle between vessel wall and nozzle wall for 90° crack location
σ_{θ}	Value of hoop stress in vessel wall (kPa)

648 094

"Stress Intensity Distributions in Nozzle Corner Cracks of Complex Geometry"*

by

C. W. Smith, W. H. Peters, W. T. Hardrath and T. S. Fleischman

INTRODUCTION

Cracks located at the inside juncture of inlet or outlet nozzles w h reactor pressure vessels still pose a difficult and only partially solved three dimensional fracture analysis problems. However, advances in the development of the high speed digital computer have opened the way for analysts to develop and refine a number of numerical techniques (i.e. finite element, boundary integral, influence function, finite difference, alternating and hybrid methods) for obtaining estimates of stress intensity factor (SIF) distributions in three dimensional (3D) cracked body problems such as the nozzle corner crack. Significant improvements in convergence have resulted. However, computer code verification is still important in order to insure that assumptions and restrictions factored into the problem formulation are, indeed, not contrary to real behavior.

Over the past decade the first author and his associates have evolved a technique consisting of a marriage between frozen stress photoelasticity and the field equations of linear elastic fracture mechanics (LEFM) for providing estimates of SIF distributions in 3D cracked body problems. The method is based upon an idea of G. R. Irwin [1] and was first applied by the first author in 1970 [2]. Since that time, features of the method have been examined in some detail [3]-[9] and

*-Research performed by the Department of Engineering Science and Mechanics of Virginia Polytechnic Institute and State University under Subcontract No. 7015 under Contract No. W-7405-Eng-26 with Union Carbide Corp.

the method has been refined to its present form [10]. After demonstrating its applicability to cracked models of the Intermediate Test Vessel, [11], the first author and his associates applied the method to a study of nozzle corner cracks in models of a boiling water reactor (BWR) pressure vessel. This study is described herein. Before presenting results of the current study, a brief review of the method is appropriate.

ANALYTICAL CONSIDERATIONS

Analytical Background - A Brief Review

For the case of Mode I loading, one begins with equations of the form:

$$\sigma_{ij} = \frac{K_I}{r^{1/2}} f_{ij}(\theta) + \sigma^o_{ij} \qquad (1)$$

for the stresses in a plane mutually orthogonal to the flaw surface and the flaw border, referred to the set of local coordinates shown in Figure 1, where the terms containing K_I, the SIF, are identical to Irwin's Equations for the plane case, and σ^o_{ij} represent the contribution of the (non-singular) stresses to the stress field in the measurement zone. The σ^o_{ij} are normally taken to be constant with r and θ at a given point along the flaw border, but they may vary from point to point. Observing that the near crack tip stress fringes tend to spread approximately normal to the flaw surface (Figure 2), Eqs. 1 are applied along $\theta = \pi/2$ (Figure 1), in conjunction with

$$\tau_{max} = 1/2\ [(\sigma_{nn}-\sigma_{zz})^2 + 4\sigma_{nz}^{\ 2}]^{1/2} \qquad (2)$$

which, when truncated to the same order as Equations (1), leads to the two parameter Equation:

$$\tau_{max} = \frac{A}{r^{1/2}} + B, \text{ where } \begin{array}{l} A = K_I/\sqrt{8\pi} \\ B = f(\sigma^o_{ij}) \end{array} . \qquad (3)$$

648 096

Eq. (3) can be rearranged into the normalized form

$$\frac{K_{AP}}{q(\pi a)^{1/2}} = \frac{K_I}{q(\pi a)^{1/2}} + \frac{f(\sigma_{ij}^{o})(8)^{1/2}}{q} \left(\frac{r}{a}\right)^{1/2} , \qquad (4)$$

where $K_{AP} = \tau_{max.}(8\pi r)^{1/2}$, q is the remote loading parameter (such as uniform stress, pressure, etc.) and a the characteristic flaw depth. In addition, τ_{max} can be determined from the Stress-Optic Law,

$$\tau_{max} = Nf/2t' \qquad (5)$$

where N is the stress fringe order, f the material fringe value and t' the slice thickness in the t direction. Equation (4) indicates that, within the zone dominated by Equations (1), with σ_{ij}^{o} as described above, a linear relation exists between the normalized apparent stress intensity factor and the square root of the normalized distance from the crack tip. Thus, one need only locate the linear zone in a set of photoelastic data and extrapolate across a very near field non-linear zone [10] to the crack tip in order to obtain the SIF. An example of this approach using data from the nozzle tests described here is given in Figure 3.

Frozen Stress Method Applied to Cracked Bodies

The frozen stress method was introduced by Oppel [12] in 1937. It capitalized upon the observation that certain transparent materials exhibit both birefringent and mechanical diphase behavior. Such materials respond to load in an anelastic manner when loaded at room temperature but above a certain temperature, called "critical", the anelastic effect is suppressed and the material becomes linearly elastic and incompressible i.e. (Poisson's Ratio → 0.5). All loads are applied above critical temperature and bodies are then cooled under load, "freezing" in both the deformation and fringe patterns obtained above critical temperature. Above "critical", the material modulus is typically 1% of its room temperature value and the material fringe value is typically 4% of its room temperature value.

Starter cracks are produced in the following way. A sharp blade is fixed in contact with and normal to the surface of the body at room temperature (or below) at the desired initiation locus and is struck, producing a small crack under the blade. This crack grows when loaded above critical temperature and takes the shape which apparently tends to minimize the SIF gradient along the flaw border. When the crack reaches its desired size, the load is reduced to stop growth and cooling is carried out. The load is removed at room temperature with negligible recovery.

EXPERIMENTS

Scale photoelastic models of the BWR geometry, each containing two diametrically opposite nozzles, were constructed, employing the dimensions given in Figure 4. A photograph of such a model showing the glue lines connecting the assembled parts is shown in Figure 5a together with a close-up view of a nozzle. Field observations suggested that starter cracks could be located in radial planes at various locations around the nozzles. In the present study, cracks in three such locations, pictured in Figure 5b, were investigated. For each position (0°, 45°, 90°) small starter cracks were inserted and enlarged above critical temperature (approximately 104°C) with internal pressure. When sufficient crack size was achieved, the pressure was reduced to stop flaw growth and the models were cooled under the reduced pressure. After unloading, slices were removed parallel to the n-z plane at intervals along the flaw border (Fig. 6), coated with matching index fluid, and analyzed in a crossed circular polariscope with white light, using the Tardy Method and reading tint of passage at about 10X. These data were fed into a simple least squares computer program for estimating the SIF distributions along the flaw borders.

RESULTS

All of the cracks that were initiated from position 0° (Figure 5b) remained in their initial planes and took the shapes shown in Figure 7. Also shown are quarter ellipses with semi-axis dimensions the same as the real cracks. These shapes reveal the following.

i) The small cracks are longer along the nozzle than along the vessel wall and bulge outward in their central portions beyond a quarter elliptic shape.

ii) Deep cracks are longer along the vessel wall than along the nozzle wall and are flattened inside a quarter elliptic shape in the central portion. These results clearly show non-self-similar flaw growth. SIF distributions corresponding to these flaw shapes are pictured in Figure 8. Only one slice was obtained for the smallest crack (0). It is interesting to note how the SIF distribution changes from concave to convex as the flaw grows deeper.

In contrast to the 0° crack shapes, Figure 9 shows that the 90° crack shapes all tended to bulge outward in the central portion and the corresponding SIF distributions shown in Figure 10 remain convex throughout the range of flaw growth.

The crack shapes formed by the growth of the starter cracks at θ = 45° produced non-planar flaw surfaces as indicated in Fig. 11. In general, the flaw turned at the vessel wall through an initial angle γ towards a plane perpendicular to the vessel hoop stress, and as the crack grew, $\gamma \rightarrow 45°$ or the crack plane approached the plane normal to the hoop stress. The portion of the flaw in the nozzle wall remained in (or near) the initial flaw plane. No significant flattening of the crack front was detected in the central region of these flaws. However, the shallow flaws exhibited a tendency to grow as two different cracks, producing a discontinuity at point P (Figure 11) along the crack front. These shallow flaw shapes exhibited convex SIF distributions along the flaw border (XIVA, XIIIB, XIIIA, in Figure 12). However, as the crack growth increased, the flaw border discontinuity (P) disappeared and the two cracks merged into a single non-planar flaw. These deeper flaws exhibited concave SIF distributions (XIIB, XIVB in Figure 12). Measurements used for a and T for these flaws are shown in Figure 11.

DISCUSSION OF RESULTS

Flaws oriented at 0° - Because it is considered the most critical case, flaws in the 0° orientation have received the most attention in the literature. Numerical estimates of SIF values have been made [13] for very shallow flaws of prescribed simple flaw shape, as well as for quarter circular [14][15][16], straight front [17] and quarter elliptical [18] flaws over larger depth ranges. Experimental studies are also available on cracks in both thick [19][20][21] and thin [22][23] walled vessels. Some analyses [14] predicted concave SIF distributions along the flaw borders and others [17] predicted convex SIF distributions. One analysis [18] predicted both types of SIF distributions. As shown, in Figure 8, the distributions can be reversed as a result of changes in the relative flaw size and shape during flaw growth.

Two of the above analyses have received substantial attention from the reactor technology community in the U.S.A. The first one [15], due to Gilman and Rashid, employs quarter circular flaw shapes, assumes self-similar flaw growth and utilizes a compliance like finite element approach in order to compute an average SIF for a given flaw size. The second analysis [16], due to Besuner and his associates, utilizes an influence function approach in order to estimate average SIF values for the same flaw geometry studied by Gilman and Rashid. The latter technique, however, can be applied to other flaw shapes.

In Figure 13 we compare the average experimental results with those of [15] and [16]. By plotting results in this manner, the influence of crack size is normalized out. The analyses appear conservative for shallow flaws when compared with experimental results from this study.

One of the analyses [18] employed quarter-elliptic flaw shapes, and although the geometry consisted of a nozzle in a flat plate, tension-tension fatigue tests were run on A508 and A533 reactor steel models in order to obtain actual flaw shapes and sizes. In a separate study, [24] the authors found that their technique of growing cracks under monotonic loading above critical temperature produced flaw shapes in photoelastic plate-nozzle models virtually identical to those generated by fatigue in geometrically similar steel models. Subject to delineation of constraints necessary to maintain such similarity, this finding suggests the potential of the method for independent determination of both flaw shapes and SIF distributions for complex 3D cracked finite body problems where neither are known a-priori.

Flaw oriented at 90° - The authors are aware of only one analysis

648 101

which predicts SIF values for this flaw orientation and that is Ref. [16]. Figure 14 presents a comparison between the theory of [16] with the data obtained in this study. Again, the analysis appears to be conservative for shallow flaws.

It is of interest to note that a given pressure produces a SIF level for 0° oriented flaws which is about three times the level for 90° oriented flaws of the same size (Figure 15). If one conjectures that this ratio should lie between the ratio $(\sigma_1)_{0°}/(\sigma_1)_{90°} = 1$ for a pressurized nozzle and $(\sigma_1)_{0°}/(\sigma_1)_{90°} = 5$ for a flat plate with a hole in a biaxial stress field ($\sigma_{max}/\sigma_{min} = 2$) the result of Figure 15 appears realistic.

<u>Flaw oriented at 45°</u> - Since the 0° and 90° flaws were initially in principal planes of the nozzle and vessel, and tended to remain there, they suggest a preference of the crack for a Mode I type of extension. The 45° flaws also exhibited this preference but they had to reorient themselves, especially near the vessel boundary during growth. In each case $\gamma \to 45°$ as the flaw grew deeper and, for the case (XIIA) where the flaw grew through the juncture, γ reached 45°, meaning that the crack aligned itself with the plane normal to the vessel hoop stress as it extended as a through crack (Figure 16). In growing and reorienting itself near the vessel wall, the normalized SIF increased from 5 to over 35, as indicated by the results for cases XIII-B and XIV-B shown in Fig. 12. In fact, when the flaws changed from the dual shape to the single shape, significant changes in the SIF occurred all along the flaw border, but the greatest SIF increases occurred near the vessel inside surface. Averaged experimental SIF values along the flaw border are plotted together with the results of [16] in Figure 17. It should be noted that

the experimental flaw geometries are quite different from the quarter circular planar flaw studied analytically in [16]. Consequently, one would not necessarily expect any degree of correlation here. The important point is that the three shallow flaws seem to behave quite differently from the two deeper ones. It would be of interest to establish more precisely the a/T range over which this change occurs.

The behavior of these flaws suggests that, when cracks occur in planes other than principal planes of stress, the presence of a shear mode will cause the crack to reorient itself in order to eliminate this mode.

SUMMARY

A series of frozen stress photoelastic experiments (14 models, 28 nozzles) were conducted on scale models of a BWR vessel geometry containing diametrically opposite cracked nozzles. Loads were static internal pressure and flaws were naturally grown under pressure from starter cracks initially oriented at 0°, 90° and 45° to a diametrial plane normal to the vessel hoop stress direction.

Both flaw shapes and SIF distributions were obtained for 21 of the nozzles. Average values from the latter were compared with analytical estimates from numerical models. Results suggest the following observations:

i) Flaws initially located in principal planes of the vessel tend to grow in those planes. Growth of the 0° flaws is non-self similar with a flattening of the central region of the flaw beginning at an a/T $\approx$ 0.4. Moreover, the SIF distribution along the 0° flaws varies from

648 103

concave for shallow flaws to convex for deep flaws. The 90° flaw growth is also non-self similar but without "flattening" in the central region. SIF distributions were all concave for the 90° flaws.

ii) For the same size flaws and pressures, the 0° flaws showed SIF values about three times the 90° flaw values.

iii) When compared to analytical models which employed quarter circular crack shapes to obtain single SIF values for each crack, the averaged experimental results suggested that the analyses were conservative for the shallow flaws.

iv) The flaws initially oriented at 45° exhibited a complex growth pattern with two distinctly different growth regimes. Below $a/T \approx 0.30$, growth remained in the original flaw plane near the nozzle wall, but took place in a continuously changing direction near the vessel inside surface, with the crack plane approaching the plane normal to the vessel hoop stress. This growth produced two non-planar crack segments, joined at a discontinuity along the crack front and which appeared to grow at different rates. Convex SIF distributions were observed for these cracks. Above $a/T \approx 0.45$ the two segments merged, forming a single non-planar flaw without a flaw border discontinuity, having a concave SIF distribution and a continuously increasing SIF near the vessel wall.

Two important conclusions are suggested by the above observations:

1) The 0° flaw orientation results show the slowest growth in the central region where the SIFs are the greatest, for moderate to deep cracks. This suggests the presence of what may be conjectured to be a stress induced constraint variation [24][25].

2) The 45° flaw results suggest that flaws will reorient them-

648 104

selves into complex surfaces in order to eliminate shear modes. Such shape changes radically alter the SIF distributions along the flaw borders.

The experimental technique does have its limitations, since the models exhibit the elastic behavior of an incompressible material. However, for problems dominated by geometric effects, with only small scale yielding and fatigue crack growth at stress ratios near unity, the authors believe that standard engineering accuracies (say ± 5%) can be expected for flaw shapes and SIF distributions, for homogeneous, isotropic materials.

ACKNOWLEDGEMENTS

The authors gratefully acknowledge the suggestions of G. D. Whitman, R. H. Bryan and J. G. Merkle and the laboratory assistance of A. Andonian. The support of Oak Ridge National Laboratory under subcontract 7015 under W-7405-Eng.-26, Union Carbide Corp., is also gratefully acknowledged.

REFERENCES

[1] Irwin, G. R. Discussion Proceedings of the Society for Experimental Stress Analysis, Vol. 16, No. 1, pp. 92-96, 1958.

[2] Smith, D. G. and Smith, C. W., "A Photoelastic Investigation of Closure and Other Effects Upon Local Bending Stresses in Cracked Plates", International Journal of Fracture Mechanics, Vol. 6, No. 3, pp. 305-318, September 1970.

[3] Schroedl, M. A. McGowan, J. J. and Smith, C. W., "An Assessment of Factors Influencing Data Obtained By the Photoelastic Stress Freezing Technique for Stress Fields Near Crack Tips", Journal of Engineering Fracture Mechanics, Vol. 4, No. 4, pp. 801-809, 1972.

[4] Smith, C. W., "Use of Three Dimensional Photoelasticity in Fracture Mechanics", Journal of Experimental Mechanics, Vol. 13, No. 12, pp. 539-544, December 1973.

[5] Schroedl, M. A. and Smith, C. W., "A Study of Near and Far Field Effects in Photoelastic Stress Intensity Determination", Journal of Engineering Fracture Mechanics, Vol. 7, pp. 341-355, 1975.

[6] McGowan, J. J. and Smith, C. W., "A Finite Deformation Analysis of the Near Field Surrounding the Tip of Crack Like Elliptical Perforations", International Journal of Fracture, Vol. 11, No. 6, pp. 977-987, December 1975.

[7] Smith, C. W., McGowan, J. J. and Jolles, M. I., "Effects of Artificial Cracks and Poisson's Ratio Upon Photoelastic Stress Intensity Determination", Journal of Experimental Mechanics, Vol. 16, No. 5, pp. 188-193, May 1976.

[8] Jolles, M. I., McGowan, J. J. and Smith, C. W., "Use of a Hybrid Computer Assisted Photoelastic Technique for Stress Intensity Determination in Three Dimensional Problems", Computational Fracture Mechanics, ASME (Computer Technology Committee of Pressure Vessels and Piping), pp. 83-102, June 1975.

[9] McGowan, J. J. and Smith, C. W., "A Plane Strain Analysis of the Blunted Crack Tip Using Small Strain Deformation Plasticity Theory", Advances in Engineering Science, Vol. 2, pp. 585-594, November 1976.

[10] Smith, C. W., "Stress Intensity Estimates by a Computer Assisted Photoelastic Method", Fracture Mechanics and Technology, Vol. 1, Sijthoff & Noordhoff, pp. 591-605, March 1977.

[11] Smith, C. W., Jolles, M. I. and Peters, W. H., "Stress Intensities for Nozzle Cracks in Reactor Vessels", Journal of Experimental Mechanics, Vol. 17, No. 12, pp. 449-454, December 1977.

648 106

[12] Oppel, G, "Photoelastic Investigation of Three Dimensional Stress and Strain Conditions", NACA TM 824 (Translation by J. Vanier) 1937.

[13] Hellen, T. K. and Dowling, A. R., "Three Dimensional Crack Analysis Applied to LWR Nozzle-Cylinder Intersection", International Journal of Pressure Vessels and Piping, Vol. 3, pp. 57-74, 1975.

[14] Reynen, J., "On the Use of Finite Elements in the Fracture Analysis of Pressure Vessel Components", ASME Paper No. 75-PVP-20, June 1975.

[15] Rashid, Y. R. and Gilman, J. D., "Three Dimensional Analysis of Reactor Pressure Vessel Nozzles", Proceedings of the First International Conference on Structural Mechanics in Reactor Technology, Vol. 4, Reactor Pressure Vessels, Part G, Steel Pressure Vessels, pp. 193-213, September 1971.

[16] Besuner, P. M., Cohen L. M. and McLean, J. L., "The Effects of Location, Thermal Stress and Residual Stress on Croner Cracks on Nozzles with Cladding", Transactions of the Fourth International Conference on Structural Mechanics in Reactor Technology, Vol. G, Structural Analysis of Steel Reactor Pressure Vessels, Paper No. G415, August 1977.

[17] Schmitt, W., Bartholome, G., Gröstad and Miksch, M., "Calculation of Stress Intensity Factors for Cracks in Nozzles", International Journal of Fracture, Vol. 12, No. 3, pp. 381-390, June 1976.

[18] Broekhoven M. J. G., "Fatigue and Fracture Behavior of Cracks at Nozzle Corners; Comparison of Theoretical Predictions with Experimental Data", Proceedings of the Third International Conference on Pressure Vessel Technology, Part II, Materials and Fabrication, pp. 839-852, April 1977.

[19] Smith, C. W., Jolles, M. I. and Peters, W. H., "Stress Intensities for Nozzle Cracks in Reactor Vessels", Journal of Experimental Mechanics, Vol. 17, No. 12, pp. 449-454, December 1977.

[20] Derby, R. W., "Shape Factors for Nozzle Corner Cracks", Journal of Experimental Mechanics, Vol. 12, No. 12, pp. 580-584, December 1972.

[21] Merkle, J. G., Robinson, G. C., Holz, P. P. and Smith, J. E., "Test of 6" Thick Pressure Vessels. Series 4: Intermediate Test Vessels V-5 and V-9 with Inside Nozzle Corner Cracks", ORNL/NUREG-7, Oak Ridge National Laboratory, August 1977.

[22] Smith, C. W., Peters, W. H. and Jolles, M. I., "Stress Intensity Factors for Reactor Vessel Nozzle Cracks", Journal of Pressure Vessel Technology, ASME-PVPD, No. 100, pp. 141-149, May 1978.

[23] Fujimura, T., Miyazono, S., Ueda, S., Namatame, H., Shabata, K., Isuzaki, T., Oba, T., Kawamura, R. and Matsumoto, M., "Results of Cyclic Pressure Loading Tests on JPDR Pressure Vessel Model No. 3", Japan Atomic Energy Research Institute ERDA-tr-11 NTIS, U.S. Dept. of Commerce, Springfield, Va. 22161, August 1975.

[24] Smith, C. W. and Peters, W. H., "Prediction of Flaw Shapes and Stress Intensity Distributions in 3D Problems by the Frozen Stress Method", Preprints of Sixth International Conference on Experimental Stress Analysis, pp. 861-864, September 1978.

[25] Smith, C. W., McGowan, J. J. and Peters, W. H., "A Study of Crack Tip Non-Linearities in Frozen Stress Fields", Journal of Experimental Mechanics, Vol. 18, No. 8, pp. 309-315, August 1978.

Table I

Model Dimensions & Loads

Test No.	Flaw Orientation	p(KPa)	a_v(mm)	a_N(mm)	a(mm)	a/T
0[a]	0°	4.72	1.78	3.30	1.30	0.087
I-Av.[b]	0°	3.20 ± 0.16	2.62 ± 0.13	4.06 ± 0	2.08 ± 0	0.14 ± 0
IV-B	0°	3.11	5.09	6.37	4.32	0.29
VI[a]	0°	4.72	6.35	7.11	5.02	0.33
V-A	0°	3.36	8.13	8.89	6.74	0.44
II-B	0°	2.76	10.16	10.16	7.96	0.53
II-A	0°	2.76	10.67	10.67	8.56	0.57
III-A	0°	2.62	16.51	13.72	12.19	0.81

[a]Nozzles 0 and VI were from Vessel VI

T = 15.1mm

[b]Avg. of IA, IB, VB
IIIB - Crack was non-planar
IVA - Material inhomogeneity near crack tip

Test No.	Flaw Orientation	p(KPa)	a_v(mm)	a_N(mm)	a(mm)	a/T
IX-B	90°	8.52	4.35	3.13	2.67	0.176
VII-B	90°	13.70	3.86	3.51	3.68	0.244
X-B	90°	10.30	6.30	4.70	4.30	0.287
XI-B	90°	12.90	6.50	4.80	4.50	0.301
VIII-Av.[c]	90°	12.80 ± .10	11.60 ± 0.60	7.40 ± 0.60	8.60 ± 0.30	0.57 ± .02

T = 15.1 mm

[c]Avg. of VIII-A and XI-A
VII-A, VIII-B Defective material near crack
IX-A, X-A Crack turned out of plane

Test No.	Flaw Orientation	p(KPa)	a_v(mm)	a_N(mm)	a(mm)	a/T
XIV-A	45°	3.88	2.67	4.37	2.13	0.154
XIII-B	45°	5.84	5.23	4.24	3.33	0.240
XIII-A	45°	5.84	5.56	5.00	4.09	0.291
XII-B	45°	3.86	6.60	6.25	6.02	0.458
XIV-B	45°	3.88	16.26	11.18	11.94	0.777

XII-A - Crack broke through surface (Figure 16)

Values of T(mm): XIV-A - 13.9 XII-B - 13.2
XIII-B - 13.9 XIV-B - 15.3
XIII-A - 14.0

648 109

Table II Test Results

0° Cracks (See Figure 8)

		$K_I/P(\pi a^*)^{1/2}$	K_I $(\frac{KPa}{\sqrt{mm}})$	α/α_{max}
0	a/T = .087	6.8	148	.500
	α_{max} = 90°			
I-AV	a/T = .14	14.1	208	.124
	α_{max} = 90°	11.4	168	.500
		14.2	209	.903
IVB	a/T = .29	19.6	280	.098
	α_{max} = 90°	18.0	258	.500
		17.0	243	.961
VI	a/T = .33	23.8	517	.126
	α_{max} = 90°	21.5	467	.500
		16.7	363	.911
VI-A	a/T = .44	27.0	417	.073
	α_{max} = 90°	23.9	370	.500
		17.7	274	.903
II-B	a/T = .53	22.8	290	.072
	α_{max} = 90°	25.9	329	.500
		22.9	291	.939
II-A	a/T = .57	24.2	307	.069
	α_{max} = 90°	27.0	343	.500
		24.3	309	.933
III-A	a/T = .81	27.2	328	.033
	α_{max} = 90°	31.5	380	.500
		29.7	358	.944

90° Cracks (See Figure 10) a^* = 6.74mm

		$K_I/P(\pi a^*)^{1/2}$	K_I $(\frac{KPa}{\sqrt{mm}})$	β/β_{max}
IXB	a/T = .176	3.37	132	.05
	β_{max} = 94°	3.34	131	.47
		3.05	120	.95
VIIB	a/T = .244	4.23	267	.05
	β_{max} = 95°	4.63	292	.47
		4.16	262	.95
XB	a/T = .287	5.51	261	.05
	β_{max} = 93°	5.95	282	.47
		4.80	228	.95

648 110

90° Cracks cont.

		$K_I/P(\pi a^*)^{1/2}$	$K_I(\frac{KPa}{\sqrt{mm}})$	β/β_{max}
XIB	a/T = .301	5.97	354	.05
	β_{max} = 95°	6.41	380	.47
		5.00	297	.95
VIIIA	$a/T\|_{av}$ = .57	8.70	512	.05
& $XIA\|_{av}$	β_{max} = 97°	9.44	556	.27
		9.77	575	.51
		9.27	546	.75
		8.77	517	.95

45° Cracks (See Figure 12) a* = 4.09mm

		$K_I/P(\pi a^*)^{1/2}$	$K_I(\frac{KPa}{\sqrt{mm}})$	β/β_{max}
XIVA	a/T = .154	6.7	93	.082
	β_{max} = 98°	15.9	221	.459
		10.1	140	.883
XIIIB	a/T = .240	7.8	163	.075
	β_{max} = 93°	20.7	433	.484
		5.4	113	.925
XIIIA	a/T = .291	8.5	178	.106
	β_{max} = 94°	21.8	456	.479
		17.3	362	.926
XIIB	a/T = .458	12.6	174	.084
	β_{max} = 94°	12.7	176	.479
		17.0	235	.948
XIVB	a/T = .777	24.1	335	.068
	β_{max} = 96°	27.3	380	.469
		28.9	402	.703
		35.4	492	.953

648 111

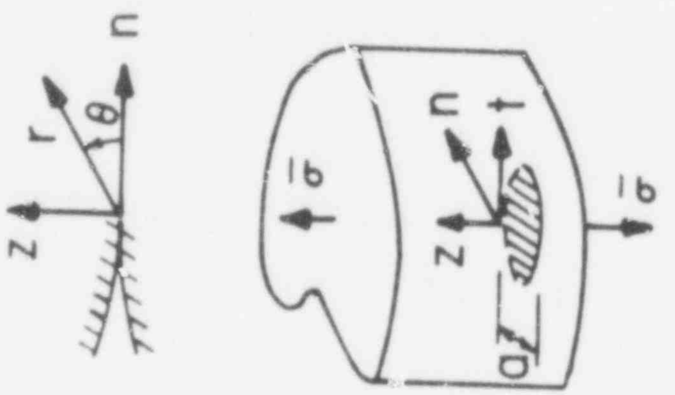

Figure 1 General Problem Geometry and Notation

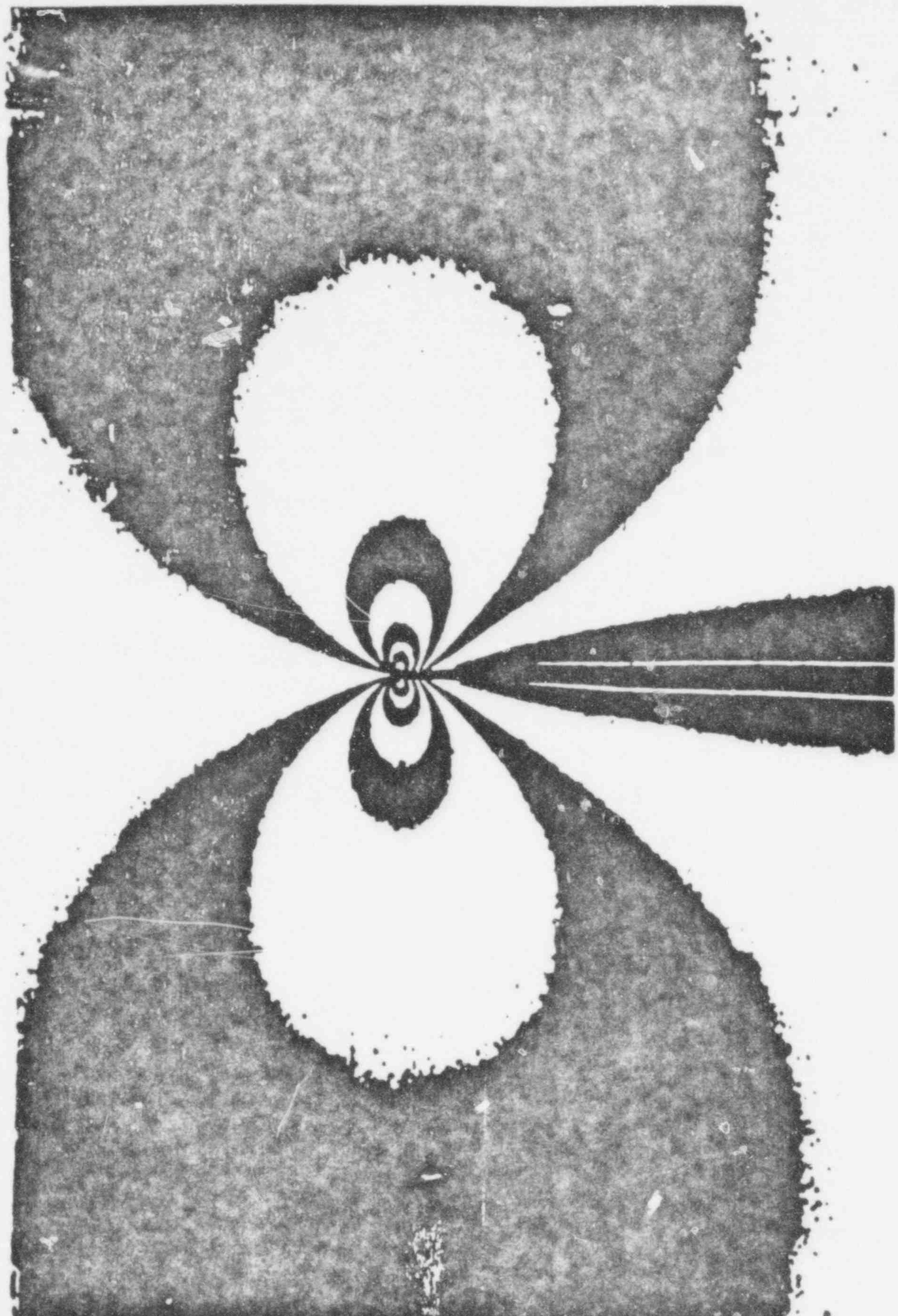

Figure 2 Local Fringe Geometry for Mode I

POOR ORIGINAL

648 113

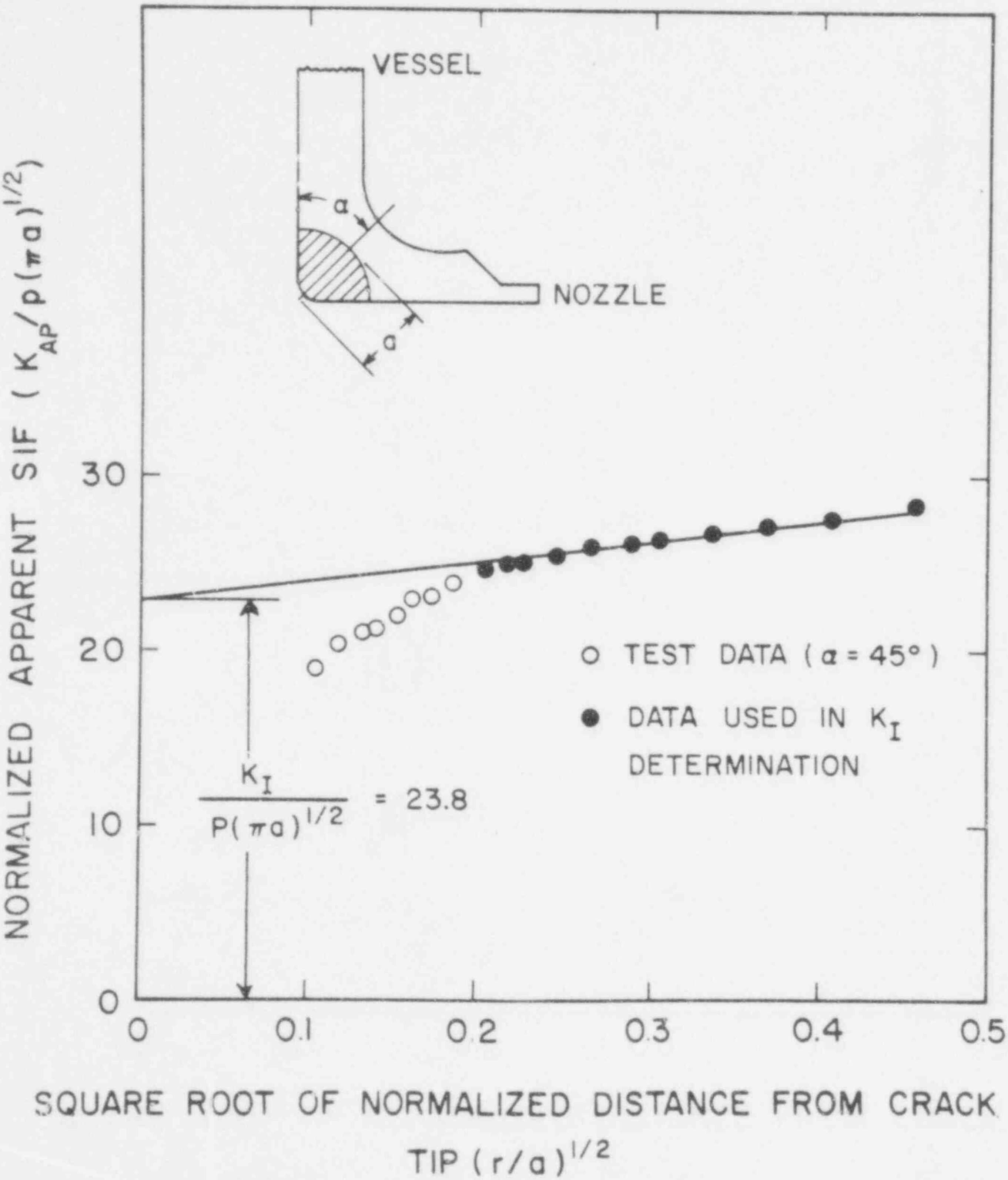

Figure 3 Typical Set of Data for Estimating SIF Value

648 114

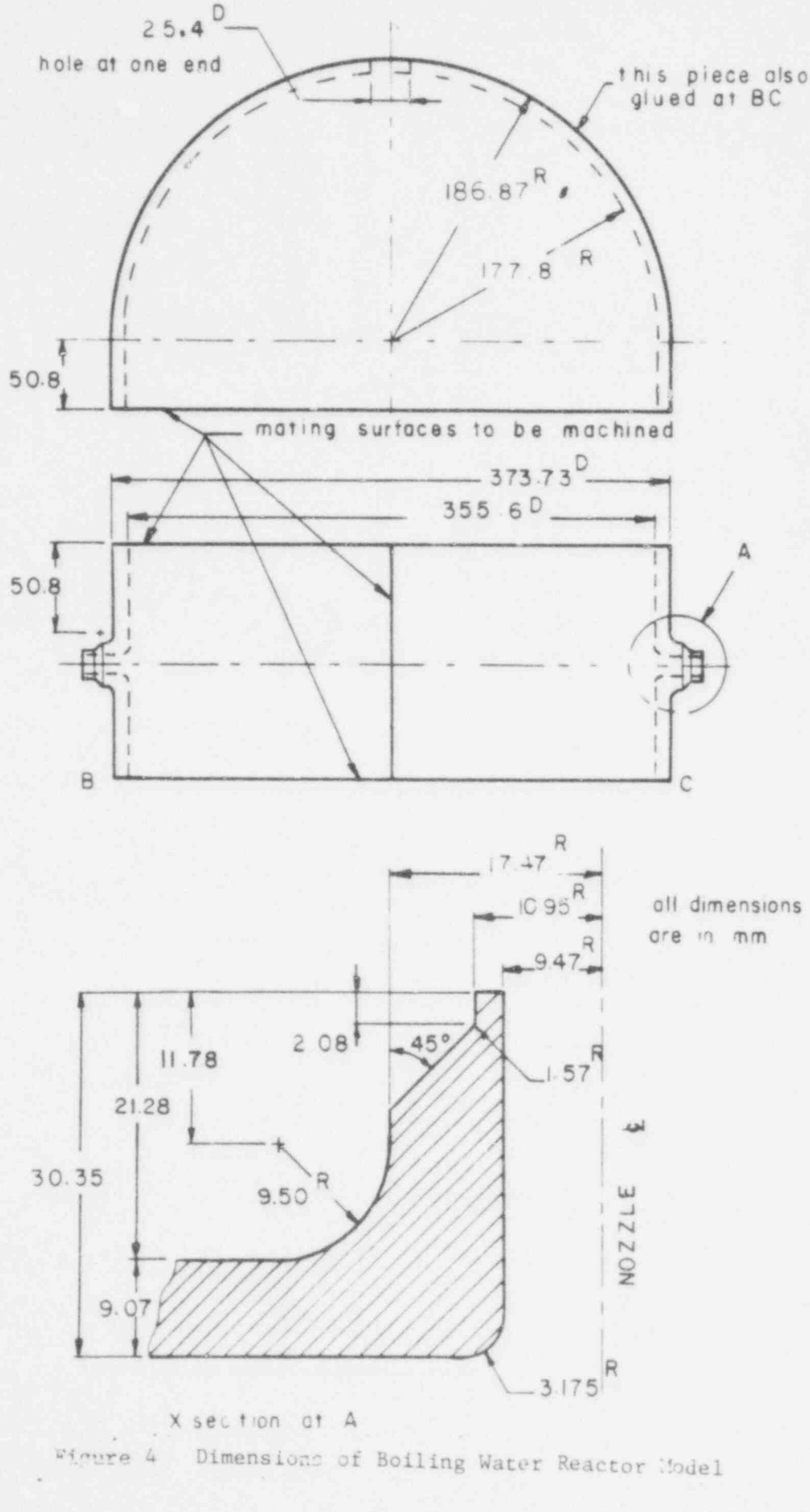

Figure 4 Dimensions of Boiling Water Reactor Model

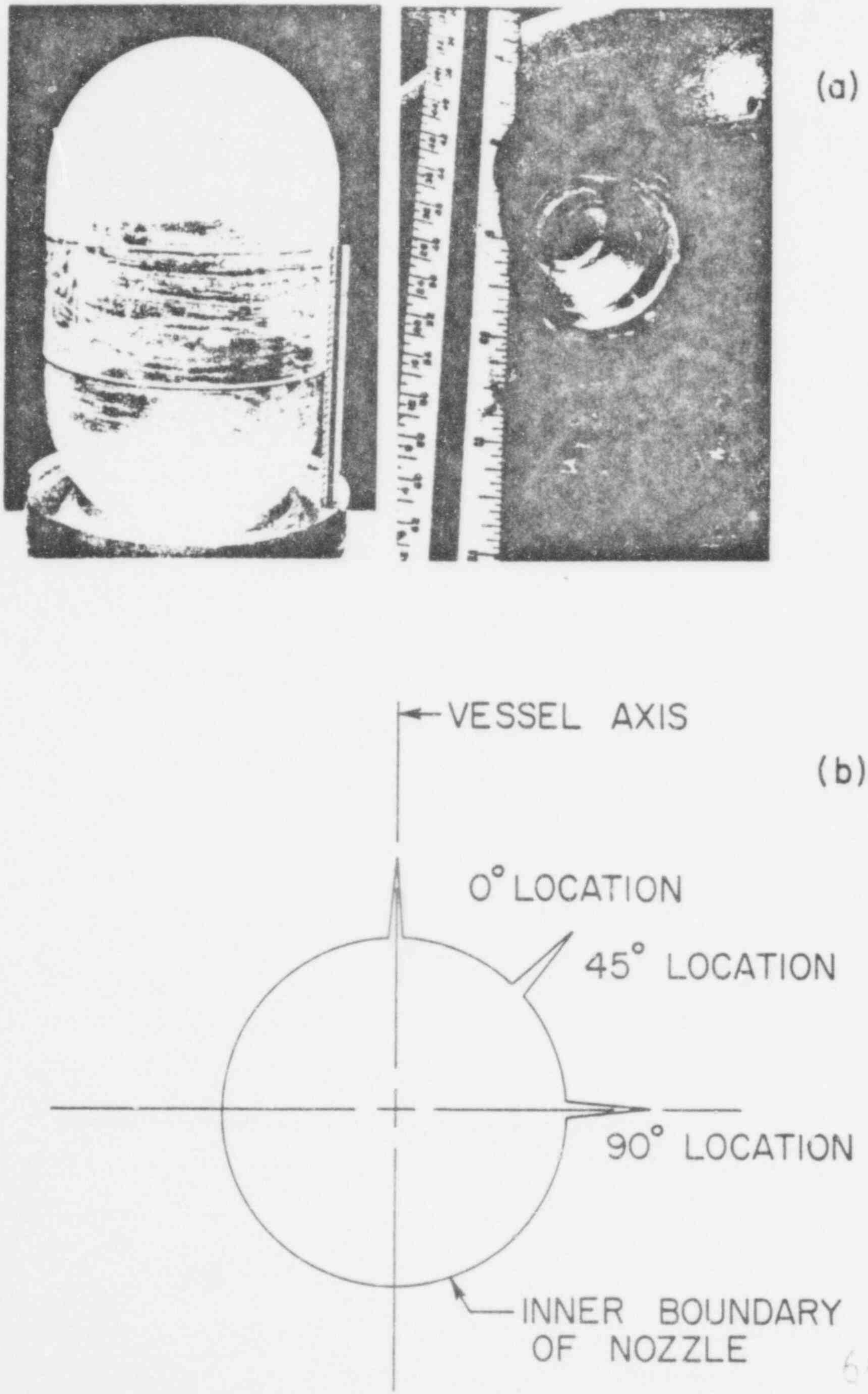

648 116

Figure 5 Photo of Model and Initial Flaw Loci Around Nozzle Boundary

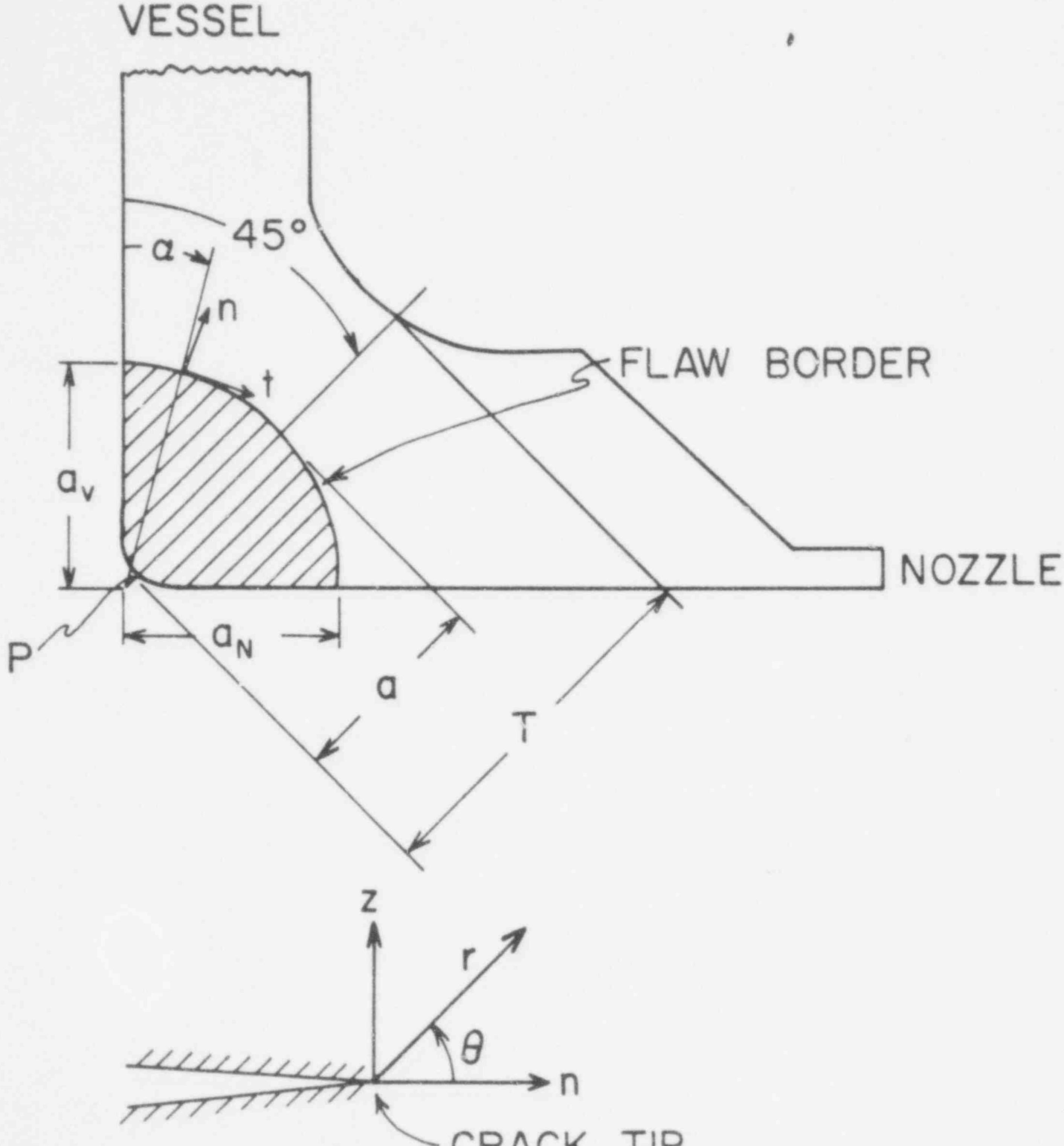

Figure 6 Problem Geometry and Notation

648 117

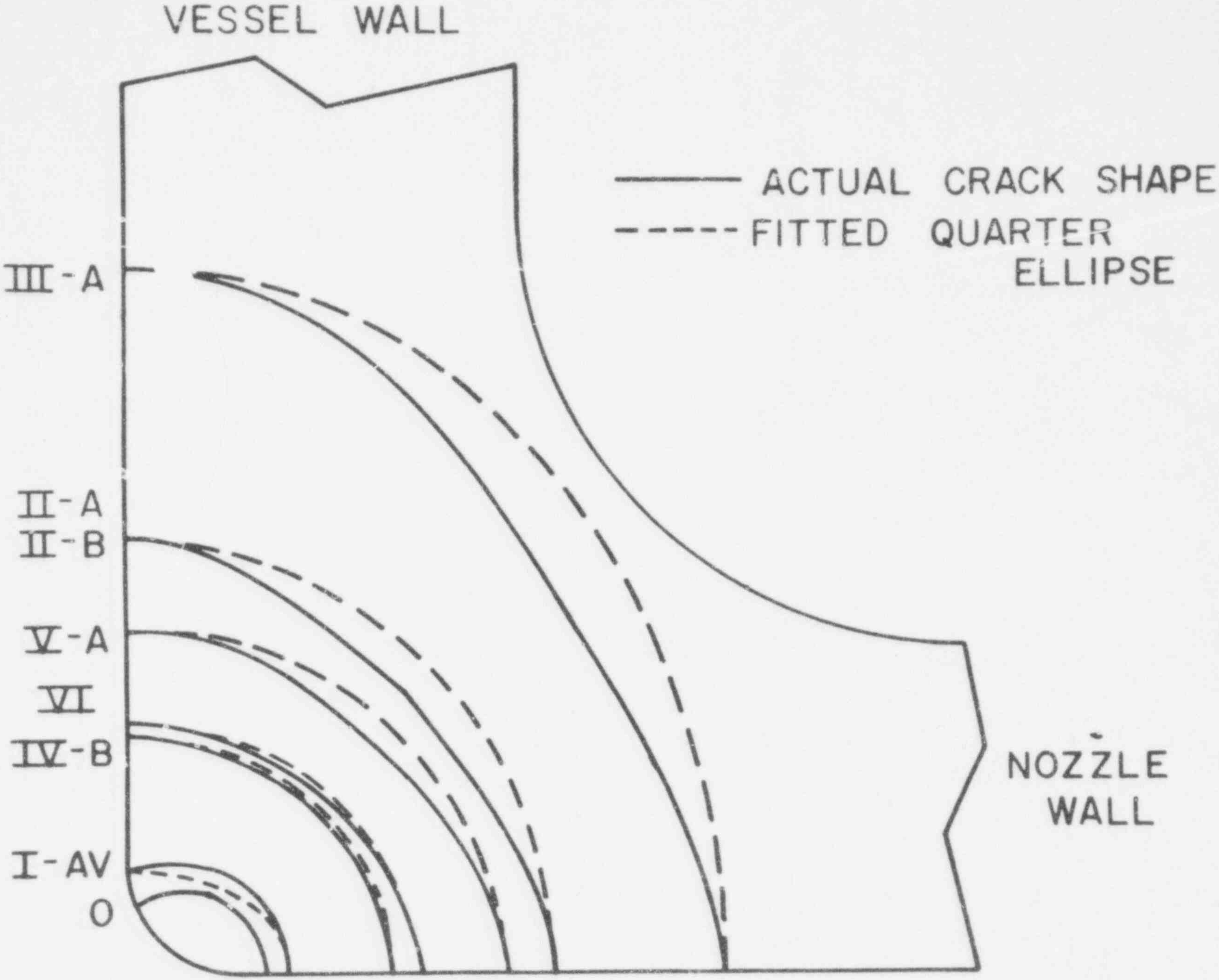

Figure 7 Flaw Shapes (0°)

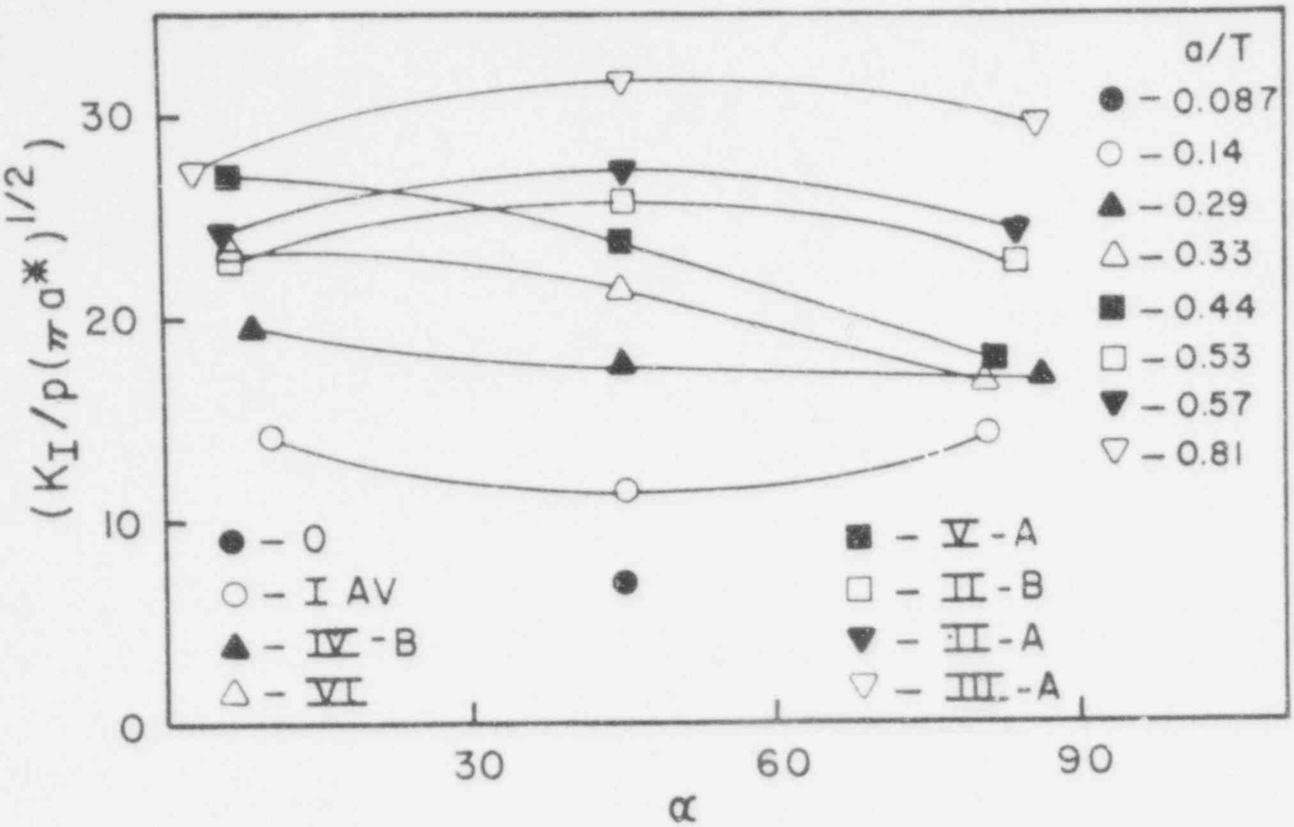

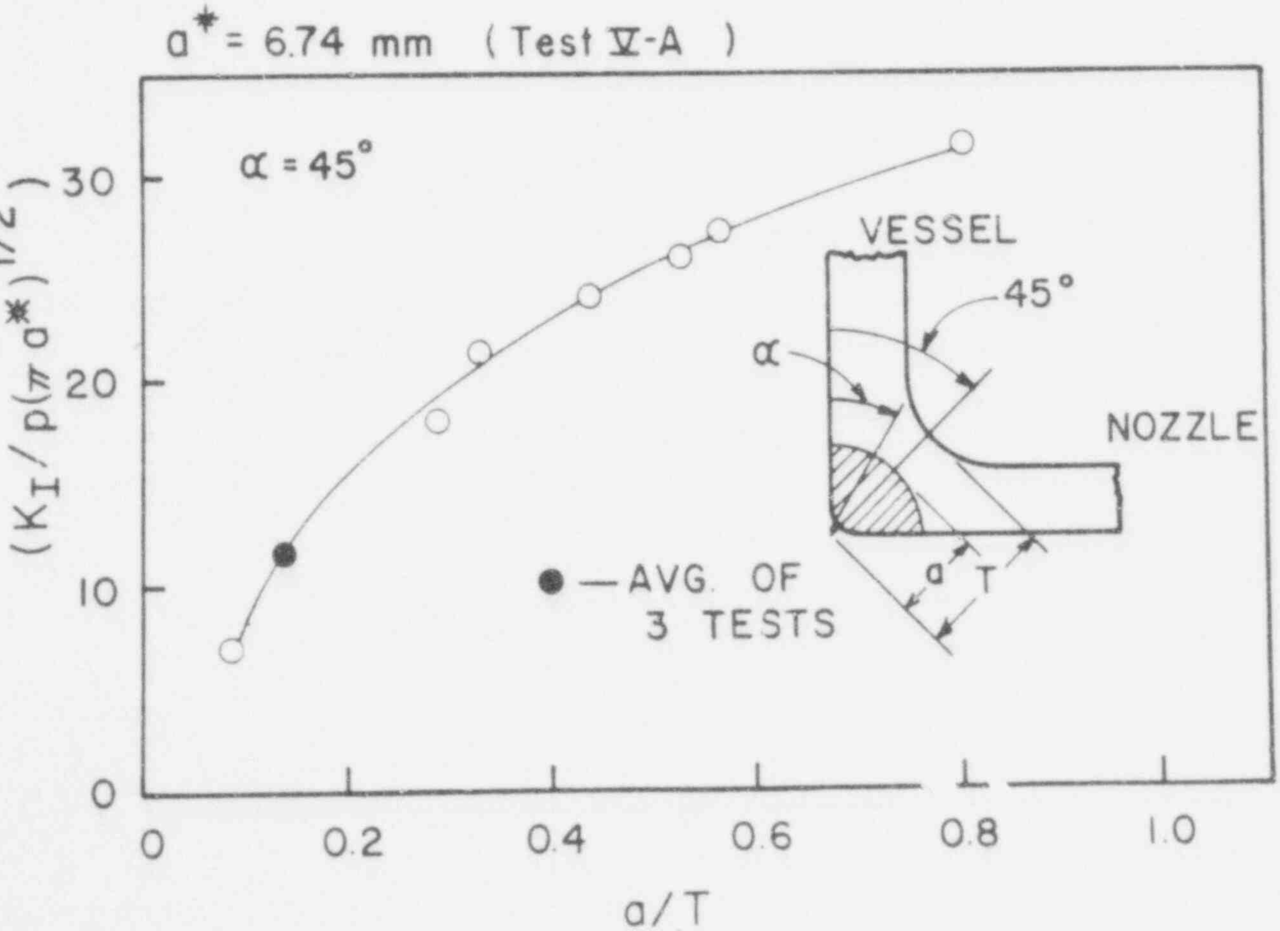

Figure 8 SIF Distributions (C°)

648 119

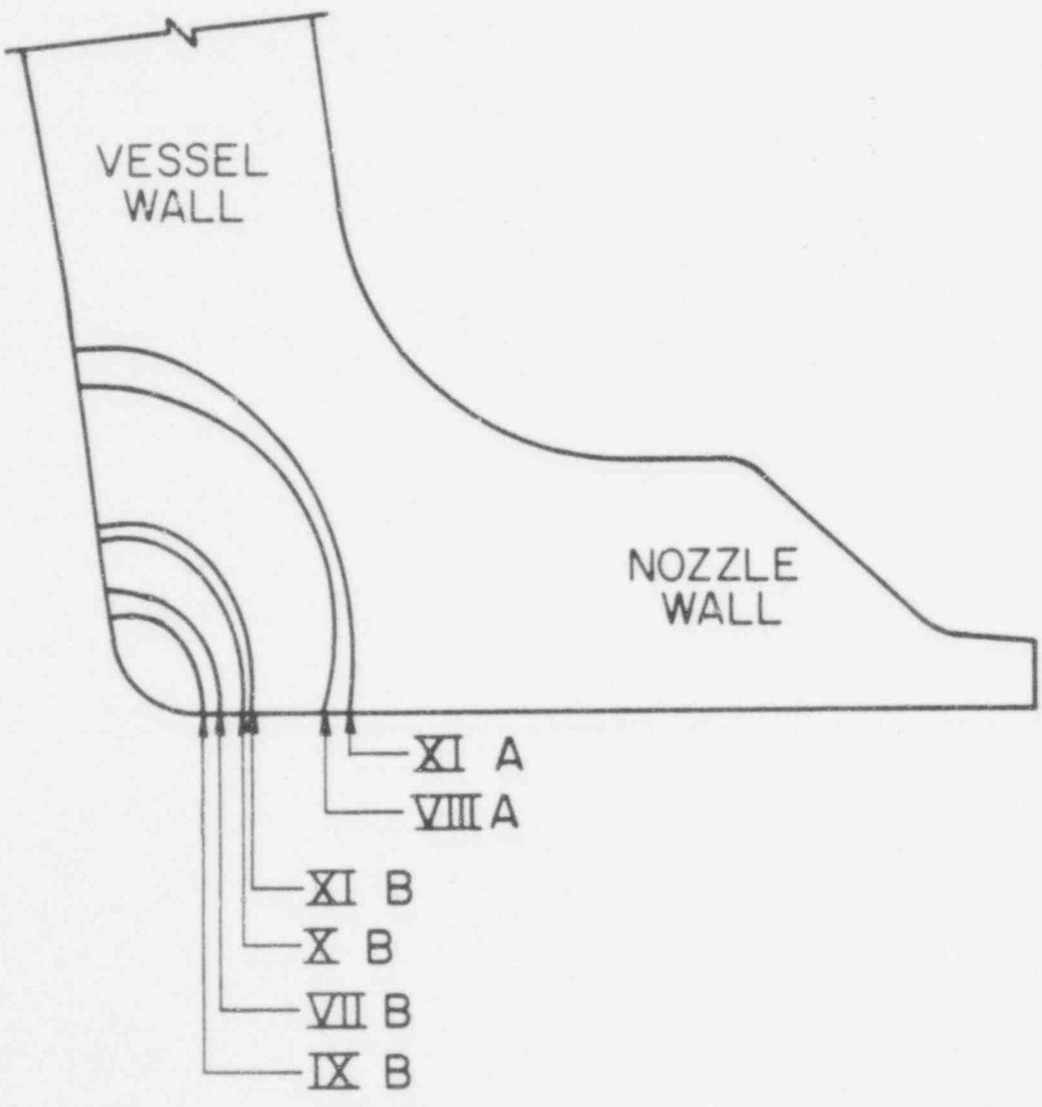

Figure 9 Flaw Shapes (90°)

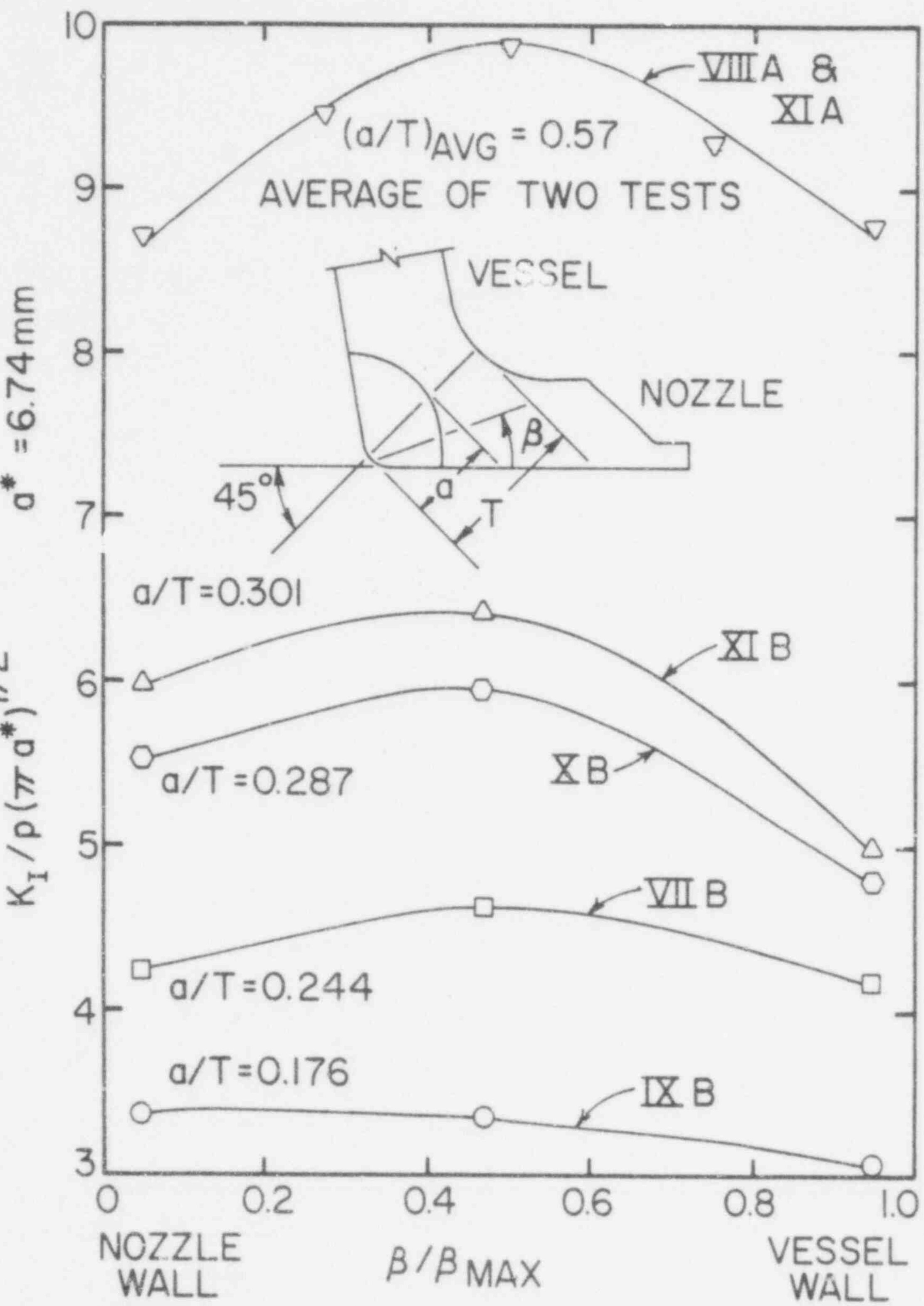

Figure 10 SIF Distributions (90°)

648 121

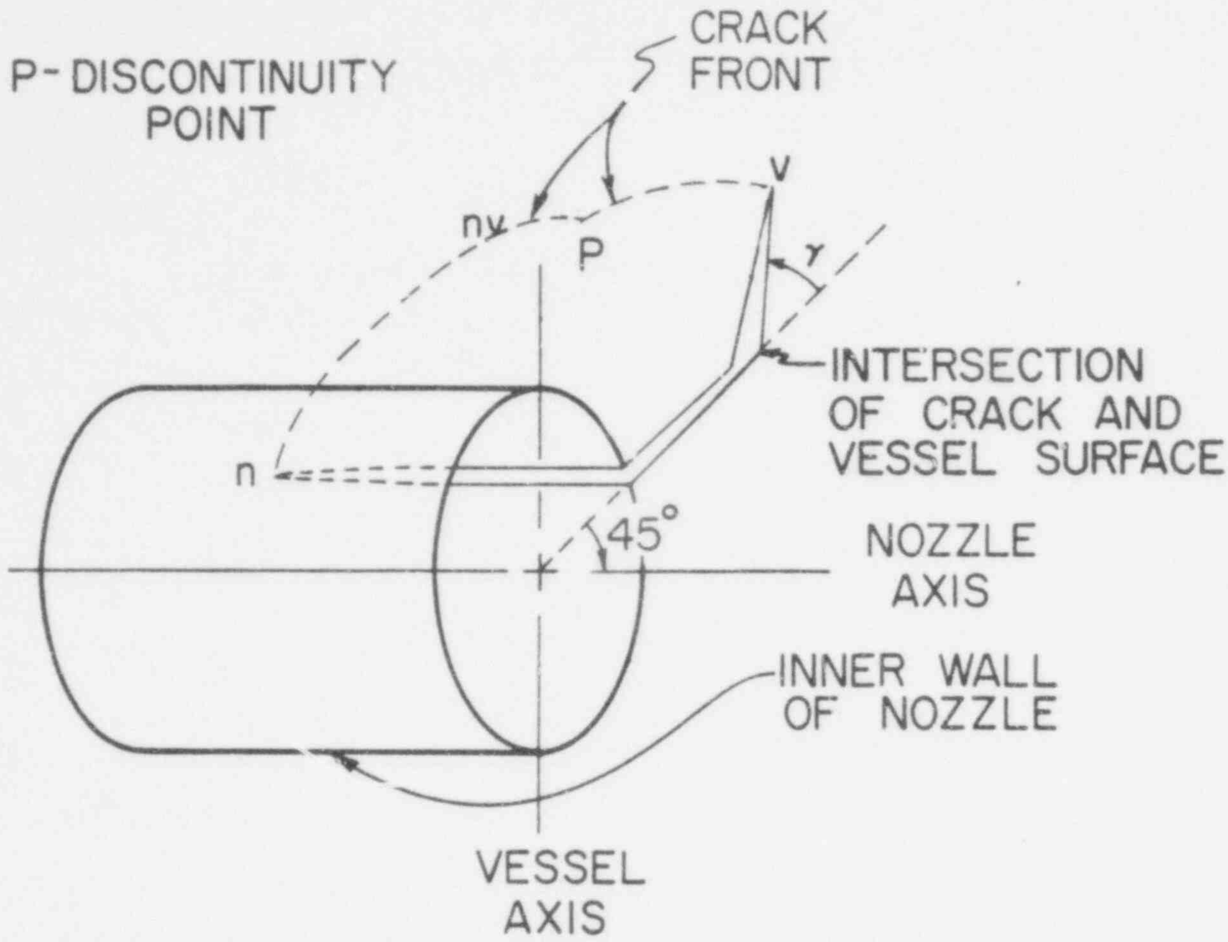

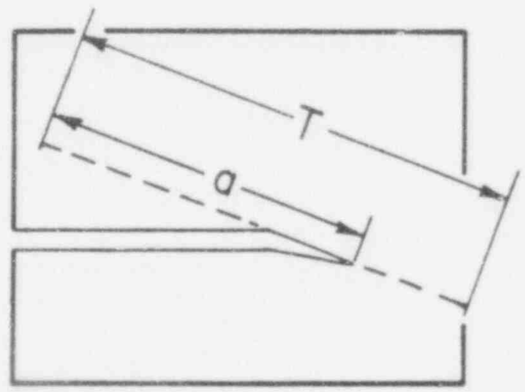

Figure 11 Flaw Shapes (45°)

648 122

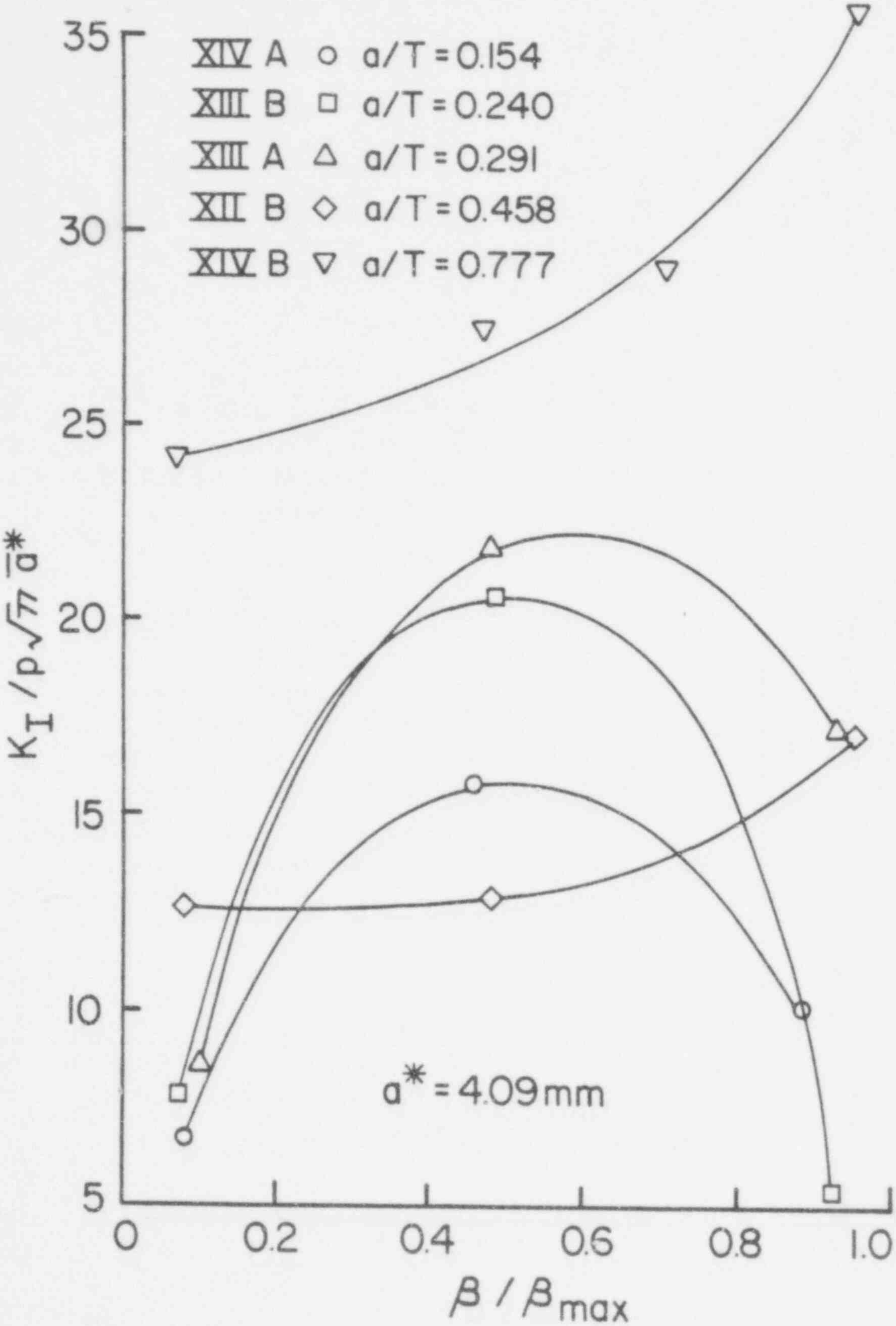

Figure 12 SIF Distributions (45°)

648 123

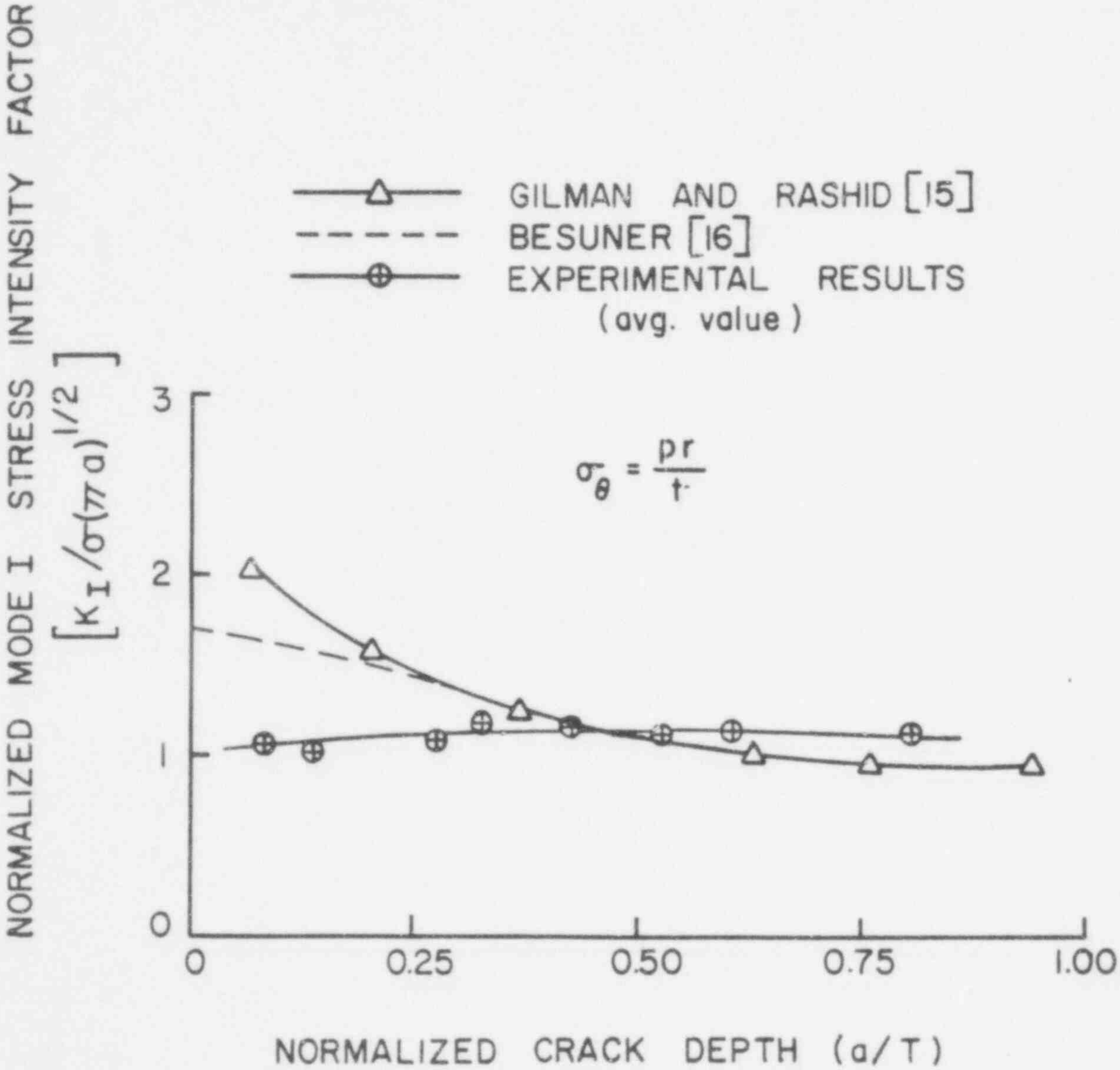

Figure 13 Comparison of Analytical and Experimental Results for Flaws with 0° Orientation

648 124

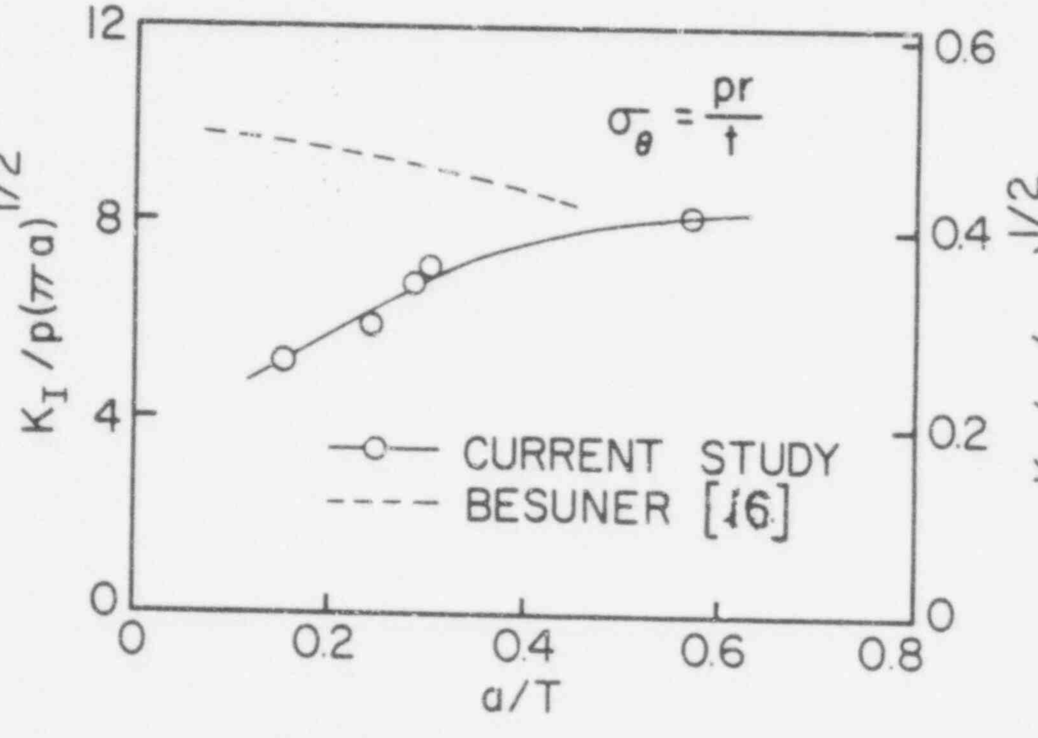

Figure 14 Comparison of Analytical and Experimental Results for Flaws with 90° Orientation

648 125

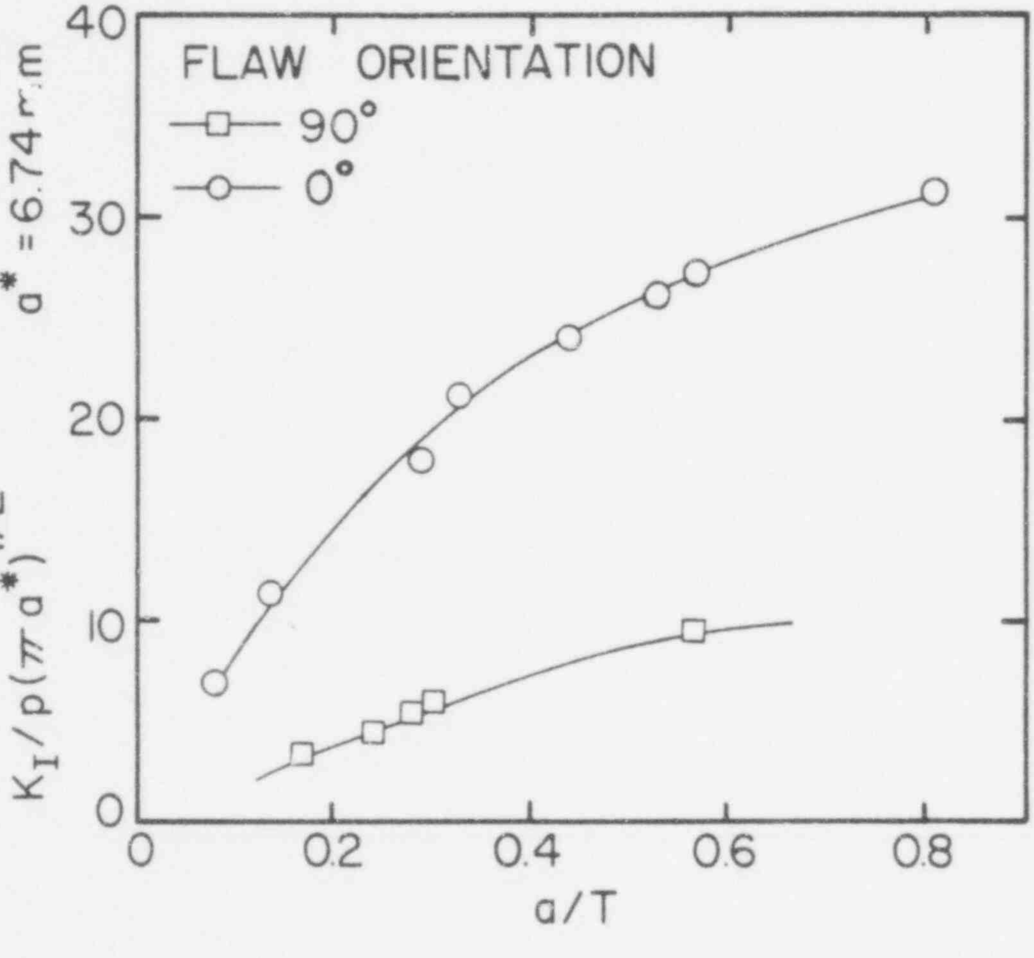

Figure 15 Comparison of Results for 0° and 90° Flaw Orientations

648 126

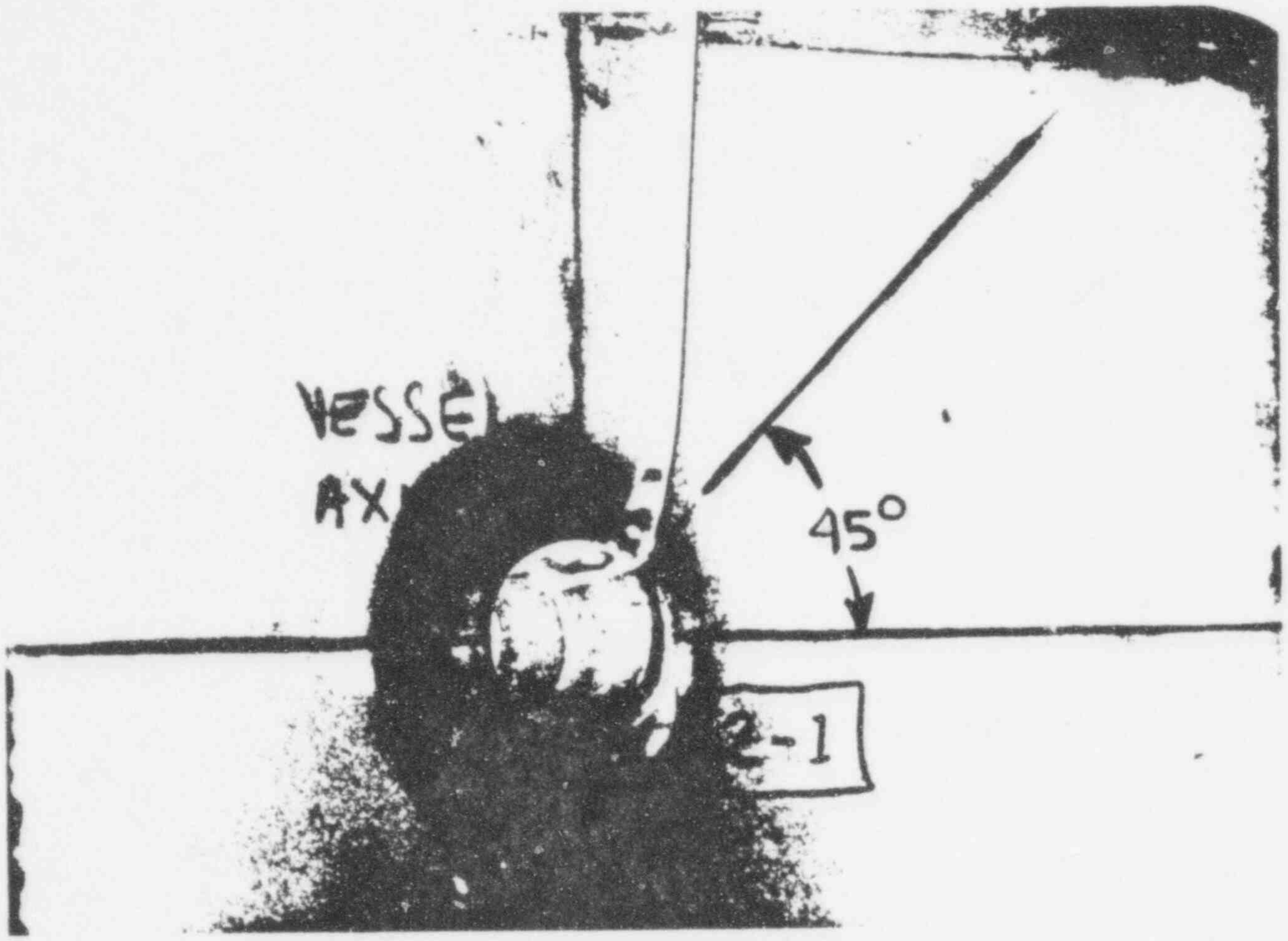

Figure 16 Photo of 45° Orientation Flaw Which Broke Through Juncture

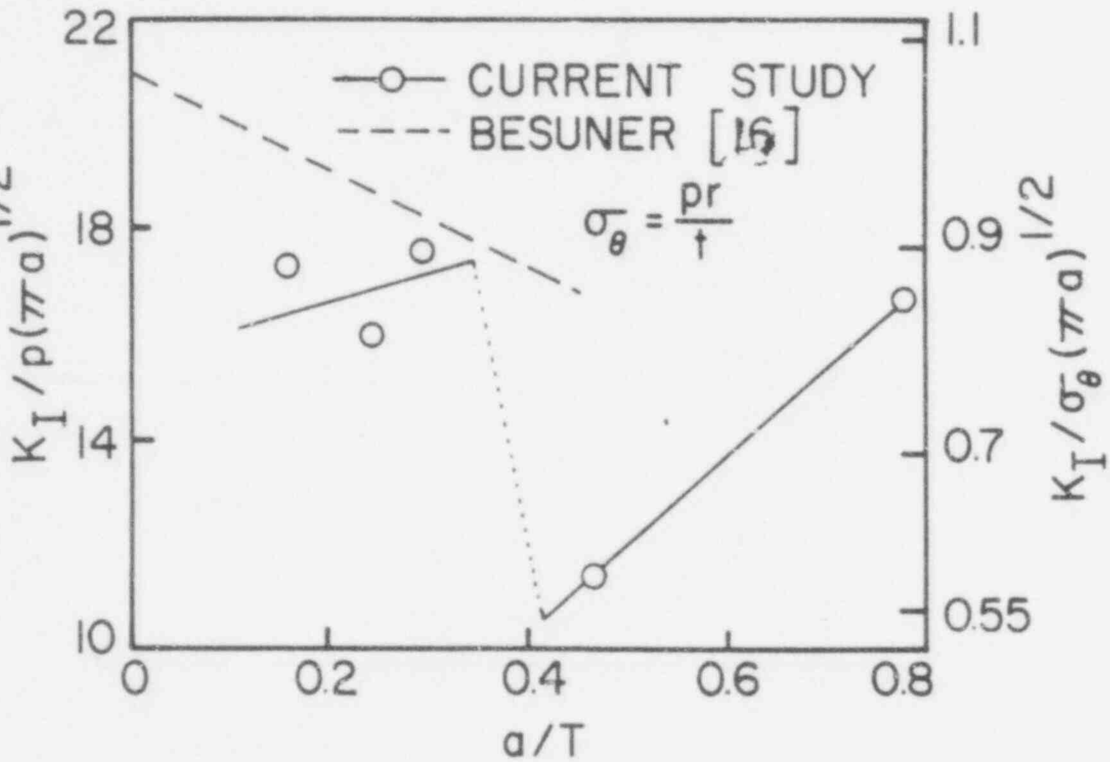

Figure 17 Comparison of Analytical and Experimental Results for Flaws with 45° Orientation

448 128

NUREG/CR-0640
ORNL/sub-7015/2
VPI-E-79-2
Dist. Category R5

Internal Distribution

1. R. G. Berggren
2. S. E. Bolt
3. R. H. Bryan
4. J. W. Bryson
5. J. P. Callahan
6. D. A. Canonico
7. R. D. Cheverton
8. J. M. Corum
9. W. B. Cottrell
10. W. L. Greenstreet
11. R. C. Gwaltney
12. P. P. Holz
13. S. K. Iskander
14. K. K. Klindt
15. Milton Levenson
16–20. J. G. Merkle
21. C. A. Mills
22. S. E. Moore
23. F. R. Mynatt
24. D. J. Naus
25. G. C. Robinson
26. G. M. Slaughter
27. J. E. Smith
28. W. J. Stelzman
29. H. E. Trammell
30–39. G. D. Whitman
40. Patent Office
41–42. Central Research Library
43. Document Reference Section
44–47. Laboratory Records Department
48. Laboratory Records (RC)

External Distribution

49. C. Z. Serpan, RSR, Nuclear Regulatory Commission, Washington, D.C. 20555
50. Office of Assistant Manager, Energy Research and Development, DOE, ORO
51–218. Special HSST distribution (by NRC)
219–511. Given distribution as shown in category R5 (NTIS-25)
512–513. Technical Information Center, P.O. Box 62, Oak Ridge, TN 37830.

648 129